JOURNAL OF THERMOPHYSICS AND HEAT TRANSFER
Vol. 8, No. 3, July–Sept. 1994

Cooled Pitot Tube in Plasma Jet: an Impact-Pressure Recovery Model

B. Porterie,* M. Larini,† and J-C. Loraud‡
Institut Universitaire des Systèmes Thermiques Industriels, Marseille 13397, France
and
L. Jestin§
Electricité de France, St-Denis 93206, France

The time-dependent axisymmetric Navier-Stokes equations are numerically integrated to predict the steady-state pressure at the forward critical point of a cooled pitot tube immersed in an air plasma flow. The flow is assumed to be in chemical equilibrium. Real gas chemistry is coupled to the gasdynamics by means of a Gibbs free energy minimization package. A Runge-Kutta multistage time integration to the central discretization of the flux balance is used. Local time stepping and residual averaging technique are used to accelerate the convergence to the steady state. Numerical results are presented for subsonic and transonic air plasma flows at four Mach numbers from 0.1 to 0.8 for gas temperature in the range of 300–5000 K. The computed values of the impact pressure are compared to values obtained from theoretical and semiempirical relations. The comparative examination indicates that the computed impact pressure is much more sensitive to the temperature difference between the gas and the pitot tube. It is found that this effect becomes greater for lower freestream Mach number which is consistent with the experimental results of Hare. Additional calculations also reveal that this effect increases as the freestream pressure decreases.

Introduction

PLASMA technology encompasses a vast area of industrial applications ranging from new material production, hazardous waste removal, semiconductor fabrication to the steel-making industry or in the metallurgy of materials like manganese.[1–3] It has direct applications in space research where the study of the thermal constraints undergone by the vehicles during their atmospheric re-entry flight is performed by simulation using air plasma flows. Its growing potential has encouraged the development of numerical modeling[4–6] as well as instrumentation to measure temperature and velocity in high-temperature jets and plasma tail flames in order to characterize their flow processes.

Beyond the temperature range of the thermocouples, optical methods based on spectroscopy[7] (from emission spectroscopy, absorption, fluorescence to Raman coherent effects), or the infrared characteristics of the plasma jet for temperature measurements and laser velocimetry for velocity measurements are difficult to use and subject to errors. As a result of this, the calorimetric enthalpy probe is the most frequently used instrument for applications in the 2500–10,000 K range.[8] This type of probe was first developed by Grey et al.[9] in the early sixties to measure temperatures and velocities in high-temperature jets and plasma tail flames. It has been used extensively and successfully for more than 25 yr in the high-temperature field.[7–27] The probe must be internally cooled to prevent destruction. To determine the temperature, the probe is used as a cooled calorimeter and the velocity is deduced from the impact pressure which is measured at the probe tip. In the latter case, the probe is used as a cooled pitot tube. To calculate the velocity from the impact pressure value, theoretical or empirical equations are generally used.

For isentropic, inviscid deceleration of an incompressible flow, the well-known Bernoulli equation is used. It links the impact pressure p_0 to the freestream flow quantities: static pressure p_∞, density ρ_∞, and velocity U_∞. It is frequently written in terms of pressure difference

$$\Delta p_1 = p_0 - p_\infty = \tfrac{1}{2}\rho_\infty U_\infty^2 \tag{1}$$

If the compressibility effects are taken into account, the pressure difference becomes

$$\Delta p_2 = p_0 - p_\infty = p_\infty \left[\left(1 + \frac{\gamma - 1}{2} M_\infty^2 \right)^{\gamma/\gamma - 1} - 1 \right] \tag{2}$$

where M_∞ is the freestream Mach number, and γ the ratio of specific heats C_p/C_v.

For viscous fluids flowing at Reynolds numbers above 100 (the Reynolds number is based on the radius of the impact tube), the viscous forces acting on the fluid are very small in comparison to the inertia forces and the above equations are valid. As the Reynolds number is decreased below 100, however, the measured impact pressure departs from the true stagnation pressure based on isentropic, inviscid deceleration, and it is no longer possible to ignore the effects of viscosity. This departure of the impact pressure from the Bernoulli pressure is known as the Barker[28] effect and has been observed experimentally by many authors.[29–31] In addition, energy transfers between the probe and the gas are very important since the gas temperature may vary from a thousand degrees to about 300 K at the surface of the probe. To account for the effects of both viscosity and heat transfer between the probe and the gas, in 1970 Carleton[18] proposed, for a plasma

Presented as Paper 92-4004 at the AIAA 17th Ground Testing Conference, Nashville, TN, July 6–8, 1992; received May 13, 1993; revision received Sept. 21, 1993; accepted for publication Oct. 1, 1993.

*Associate Professor, Department of Two-Phase and Reactive Flows, URA CNRS 1168, Université de Provence, Av. Esc. Normandie Niemen. Member AIAA.
†Professor, Department of Two-Phase and Reactive Flows.
‡Professor, Department of Two-Phase and Reactive Flows. Member AIAA.
§Research Engineer, Department REME, EdF.

flow around a hemispherically tipped cylindrical body, the following relation for the pressure difference:

$$\Delta p_3 = p_0 - p_\infty = \frac{1}{2}\rho_\infty U_\infty^2 + \frac{1}{8}\frac{\rho_\infty^2 U_\infty^4}{\gamma p_\infty} + \frac{2\bar{\mu}U_\infty}{a[1 + (0{,}5576/\sqrt{Re})]} \tag{3}$$

where a is the radius of curvature of the probe at the impact point, $\bar{\mu}$ the viscosity, and Re is the Reynolds number defined as $aU_\infty\bar{\rho}/\bar{\mu}$.

The right member is a sum of a Bernoulli term, a compressibility term, and viscous term, respectively. The viscosity $\bar{\mu}$ and the density $\bar{\rho}$ are evaluated at a reference temperature. This is taken to be the temperature corresponding to the mean boundary-layer enthalpy $\bar{h} = 0.5(h_w + h_\infty)$, where w denotes body surface conditions.

This model for pressure recovery at the stagnation point of a cool impact probe was confirmed for an argon plasma flame flowing at Reynolds number below 100 by Carleton and Kadlec[20] from their experimental results.

In 1977 Hare[23] carried out experiments where probes were immersed in low-pressure plasma tail flames. The author first compared measures obtained using a cooled pitot tube with those obtained using an uncooled ceramic probe. He then went on to measure the impact pressure using a carbon impact tube heated up to 2500 K and positioned on the axis of a turbulent nitrogen jet at 300 K. The results show quite clearly that, as argued first by Smith and Churchill[32] in 1965, the presence of a thermal boundary layer surrounding the probe tip does affect the magnitude of the measured impact pressure, and this effect becomes significant when the temperature difference between the probe and the gas exceeds 1800 K. Hare verified that none of the relations above explain the results, and concluded that until an explanation can be found, the use of cooled probes to measure velocity in high-temperature jets from the impact pressure is not recommended. In spite of these objections raised by Hare, due to a lack of any alternative, cooled pitot tubes are still widely used in different laboratories and industrial sites. However, certain scientists were worried by these objections and wished to ascertain, more precisely, the limits of such an instrument in measuring the flow velocity in air plasma torches in the range of atmospheric pressure. That is the reason why, in this article, we concern ourselves with the use of a cooled pitot tube to measure air plasma flow velocity. More precisely, this article aims at establishing an unquestionable link between the impact pressure and the freestream velocity for extreme freestream conditions in which the probe may be used, i.e.: 1) pressure in the range 0.25–1 atm; 2) temperature in the range 300–5000 K; and 3) Mach number in the range 0.1–0.8.

With this end in view, the Navier-Stokes equations are solved for a plasma flow of five-species equilibrium air. This work completes and improves on that of a former article[33] where the governing equations were solved using the well-known MacCormack's scheme for the subsonic case ($0.3 \leq M_\infty \leq 0.8$). Furthermore, it is based on a numerical method well suited to the calculation of the steady-state solution and which allows one to extend the domain of application to the low-subsonic case (up to $M_\infty = 0.1$).

In this article we first detail the theoretical model and the numerical algorithm. Then, computed impact pressure for freestream conditions given previously are presented and compared to those obtained from the relations (1–3) in order to show evidence of Hare's restraints. Computed flowfields reveal the effectiveness of the method employed which obtains an accurate steady-state solution.

Unfortunately, the experimental data used in the above-mentioned experiments cannot be used in a validation process. In the rare cases for which the precise test conditions can be deduced from the experiments these conditions are outside the applicability domain of the present numerical model.

Analysis

Governing Equations

The governing equations of the plasma flow around a pitot tube are the axisymmetric Navier-Stokes equations written in an arbitrary coordinate system $\xi = \xi(x, y)$ and $\eta = \eta(x, y)$ as (see Peyret and Viviand[34])

$$q_t = -F_\xi - G_\eta - (1/y)H \tag{4}$$

where

$$q = J^{-1}\begin{bmatrix}\rho\\ \rho u\\ \rho v\\ e\end{bmatrix}, \qquad F = J^{-1}\begin{bmatrix}\rho U\\ \rho uU + \xi_x p - \xi_x\tau_{xx} - \xi_y\tau_{xy}\\ \rho vU + \xi_y p - \xi_x\tau_{xy} - \xi_y\tau_{yy}\\ (e + p)U - \xi_x R - \xi_y S\end{bmatrix}$$

$$G = J^{-1}\begin{bmatrix}\rho V\\ \rho uV + \eta_x p - \eta_x\tau_{xx} - \eta_y\tau_{xy}\\ \rho vV + \eta_y p - \eta_x\tau_{xy} - \eta_y\tau_{yy}\\ (e + p)V - \eta_x R - \eta_y S\end{bmatrix}$$

$$H = J^{-1}\begin{bmatrix}\rho v\\ \rho uv - \tau_{xy}\\ \rho v^2 - \tau_{yy} + \tau_{\theta\theta}\\ (e + p)v - S\end{bmatrix}$$

with

$$\tau_{xx} = \tfrac{2}{3}\mu[2\xi_x u_\xi + 2\eta_x u_\eta - \xi_y v_\xi - \eta_y v_\eta - (v/y)]$$

$$\tau_{xy} = \mu(\xi_y u_\xi + \eta_y u_\eta + \xi_x v_\xi + \eta_x v_\eta)$$

$$\tau_{yy} = \tfrac{2}{3}\mu[2\xi_y v_\xi + 2\eta_y v_\eta - \xi_x u_\xi - \eta_x u_\eta - (v/y)]$$

$$\tau_{\theta\theta} = \tfrac{2}{3}\mu[-\xi_x u_\xi - \eta_x u_\eta - \xi_y v_\xi - \eta_y v_\eta + 2(v/y)]$$

$$R = u\tau_{xx} + v\tau_{xy} + kT_x$$

$$S = u\tau_{xy} + v\tau_{yy} + kT_y$$

where the derivatives of the temperature, T_x and T_y, are expanded by chain rule

$$T_x = \xi_x T_\xi + \eta_x T_\eta$$
$$T_y = \xi_y T_\xi + \eta_y T_\eta$$

In these equations, ρ, e, p, u, and v are the density, total energy per unit volume, pressure, axial, and radial velocity components, respectively.

The contravariant velocity components U and V are related to u and v by

$$U = \xi_x u + \xi_y v$$
$$V = \eta_x u + \eta_y v \tag{5}$$

Intrinsic (also called body-oriented) coordinates are used, such that ξ is the distance along the body surface, η is the distance normal to the body surface.

Here, J is the transformation Jacobian

$$J = \xi_x\eta_y - \xi_y\eta_x = (x_\xi y_\eta - x_\eta y_\xi)^{-1} \tag{6}$$

The various metric coefficients are easily formed from the derivatives x_ξ, y_ξ, etc., using the relations

$$\xi_x = Jy_\eta, \quad \xi_y = -Jx_\eta, \quad \eta_x = -Jy_\xi, \quad \eta_y = Jx_\xi \tag{7}$$

The viscosity and the thermal conductivity depend on the temperature according to data of Pateyron et al.[35]

The system is supplemented by the equations of state

$$p = \rho RT \sum_{i=1}^{N} \frac{Y_i}{m_i} \tag{8}$$

$$(e/\rho) = e_{\text{int}} + 0.5(u^2 + v^2) \tag{9}$$

with

$$e_{\text{int}} = \sum_{i=1}^{N} Y_i \left(h_{fi} + \int_{T_0}^{T} C_{pi}\, dT \right) - \frac{p}{\rho} \tag{10}$$

where e_{int}, R, T_0, h_{fi}, C_{pi}, Y_i, and m_i are the internal energy of the gas per unit mass, universal gas constant, reference temperature, heat of formation at T_0, constant-pressure specific heat, mass fraction, and molecular weight of the ith species ($i = 1, \ldots, N$), respectively.

Chemistry Coupling

For the present analysis, the Navier-Stokes equations are coupled to an equilibrium real-gas chemistry package. The equilibrium state of the gas at each mesh point is computed by minimizing the Gibbs free energy. The minimization is performed using the iterative method of Brinkley.[36,37]

Since the upper limit temperature is restricted to 5000 K, ionization and radiation of the atomic species are neglected. The primary species O_2, O, N_2, N, and NO are considered. The equilibrium constants are taken from JANAF thermochemical tables.[38]

For each diatomic species, the vibrational energy is assumed to be in thermodynamic equilibrium with the other internal energy modes. Using a simple harmonic oscillator model, the expression for the equilibrium vibrational $C_{v_{\text{vib}i}}$ is given as[39]

$$C_{v_{\text{vib}i}} = Ru_i^2 \frac{\exp(u_i)}{[\exp(u_i) - 1]^2}, \quad u_i = \frac{\theta_{\text{vib}i}}{T}, \quad i = O_2, N_2, NO \tag{11}$$

where $\theta_{\text{vib}i}$ is the so-called characteristic temperature of vibration of the ith diatomic species. Although the JANAF tables use partition functions that include anharmonic vibrational effects and electronic contributions in calculating the equilibrium constants, the simplifying assumption of a harmonic oscillator model for vibrational energy can be reasonably applied in the present analysis due to the relatively low temperature level and thermodynamic equilibrium.

Body Surface Equation

The body surface equation is assumed to coincide with the Stokes' stream surface through the stagnation point for an axisymmetric steady irrotational flow of an ideal fluid obtained by combining a uniform flow and a source at the origin. The distance of any point M on the body surface from the axis of symmetry Ox is given by

$$y^2 = \tfrac{1}{2}\omega^2(1 + \cos\alpha) \qquad \text{where} \qquad \alpha = (Ox, OM) \tag{12}$$

Here, ω is the asymptotic radius of the body as α approaches 0 (Fig. 1). In Fig. 1, a is the radius of curvature of the body at the impact point which corresponds to $\alpha = \pi$.

Computational Mesh

Figure 2 shows the computational grid about the pitot tube with 61 points in both of the two directions. The axis of symmetry is located midway between two ξ lines. Grid lines are clustered at the symmetry axis and near the body surface in order to achieve a good resolution of the flow in these regions of high gradients. From the axis of symmetry, the mesh width in the ξ direction is stretched geometrically by a factor of 1.06 for a distance of 31 mesh widths, and by a factor of 1.16 up to the downstream boundary. In the η direction, an analogous point distribution is performed from the body surface to the freestream boundary. An enlargement of the grid is also shown in Fig. 2.

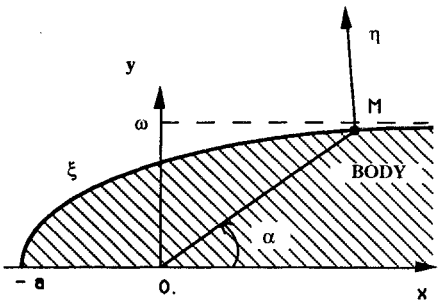

Fig. 1 Schematic of the pitot tube surface.

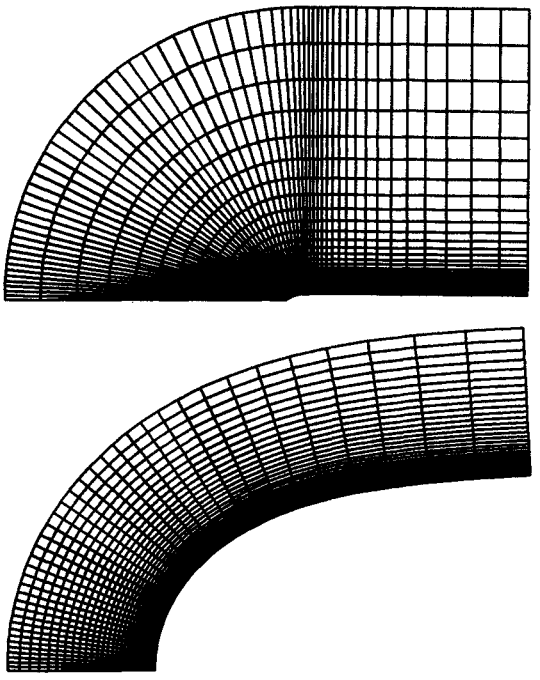

Fig. 2 61 × 61 grid for pitot tube; global view and enlargement.

Boundary Conditions

Along the body surface ($\eta = 0$), temperature is specified $T = T_p$, and the no-slip velocity boundary conditions are $u = v = 0$ (or $U = V = 0$). Due to the possible low Reynolds number of the plasma flow, the approximation of zero normal pressure gradient cannot be enforced. The pressure on the body surface can then be obtained by combining the momentum equations evaluated at the wall. One such relation is found by simplifying η_x (ξ momentum) + η_y (η momentum):

$$\begin{aligned} p_\xi(\eta_x\xi_x + \eta_y\xi_y) + p_\eta(\eta_x^2 + \eta_y^2) &= \eta_x\xi_x\tau_{xx\xi} + \eta_x^2\tau_{xx\eta} \\ &+ \eta_x(\xi_x + \xi_y)\tau_{xy\xi} + 2\eta_x\eta_y\tau_{xy\eta} + \eta_y\xi_y\tau_{yy\xi} + \eta_y^2\tau_{yy\eta} \\ &+ (1/y)(\eta_x\tau_{xy} + \eta_y\tau_{yy} - \eta_y\tau_{\theta\theta}) \end{aligned} \tag{13}$$

In the present application, subsonic flow in the far field is considered, and therefore, the boundary conditions are based on the theory of characteristics for locally one-dimensional inviscid flow normal to the boundary. The locally one-di-

mensional Riemann invariants, entropy, and tangential velocity component are given by

$$R_1 = V_f \cdot \boldsymbol{n} - \frac{2}{\beta - 1} c \tag{14a}$$

$$R_2 = V_f \cdot \boldsymbol{n} + \frac{2}{\beta - 1} c \tag{14b}$$

$$R_3 = \text{—} \left(\frac{p}{\rho^\beta} \right) \tag{14c}$$

$$R_4 = V_f - (V_f \cdot \boldsymbol{n})\boldsymbol{n} \tag{14d}$$

where V_f is the plasma flow velocity, $\boldsymbol{n}$ is the unit vector normal to the far-field boundary, and c is the local sound speed.

For a thermally or calorically perfect gas, c becomes $(\gamma p/\rho)^{1/2}$, where γ is the ratio of specific heats C_p/C_v. For a real gas, this is no longer valid. But an analogy can be made by defining c as $(\beta_p/\rho)^{1/2}$, where[40]

$$\beta = 1 + (p/\rho e_{\text{int}}) \tag{15}$$

For subsonic inflow, R_1, R_3, and R_4 are given from outside ($R_m = R_{m\infty}$, $m = 1$, 3, and 4) and R_2 from inside ($\partial R_2/\partial n = 0$).

At the symmetry axis ($y = 0$), ρ, u, and e are even functions with respect to y, and v is an odd one: $(\rho, u, v, e)^T(x, y) = (\rho, u, -v, e)^T(x, -y)$.

At the downstream boundary, the pressure is specified and the other flow variables are extrapolated.

Numerical Procedure

The scheme used to calculate the steady-state solution via a pseudotransient formulation is based on a central, second-order finite difference discretization of the flux gradients and a separate time-integration method. Following Jameson et al.,[41] Jameson,[42,43] efficient dissipation terms, convergence acceleration techniques are added to the scheme. The separate treatment of the space and time discretizations is a convenient way to assure a steady-state solution independent of the time step. This method may be extended to the Navier-Stokes equations.[44–46]

Spatial Discretization

In this method, the governing equations are first reduced to a system of time-dependent ordinary differential equations (ODEs) by using the conventional three-point centered difference discretization of the first and second derivatives, except that the derivatives of the temperature T_ξ and T_η in the terms R and S are approximated by fourth-order accurate five-point differences. The use of such high-order approximation is made in order to reduce the associate truncation error for these derivatives. These ODEs can be written as

$$\frac{\mathrm{d}q_{i,j}}{\mathrm{d}t} = R(q_{i,j}) \tag{16}$$

with the residual defined by

$$R(q_{i,j}) = -\frac{F_{i+1,j} - F_{i-1,j}}{2\Delta\xi} - \frac{G_{i,j+1} - G_{i,j-1}}{2\Delta\eta} - \frac{H_{i,j}}{y_{i,j}} \tag{17}$$

In order to control the high-frequency waves which are not damped by the scheme, the nonlinear artificial dissipation model of Jameson et al. (Jameson et al.,[41] Jameson[42,43]), extended to general curvilinear coordinates by Pulliam[47] is applied. In order to avoid deterioration of accuracy, it is necessary to reduce the artificial dissipation in the vicinity of the solid boundary by multiplication with a factor which goes quadratically to zero with Mach number.

Time Integration

A four-stage Runge-Kutta (RK) time marching scheme is applied to solve the previous ODEs. The general form of such scheme is

$$\begin{aligned} q_{i,j}^{(0)} &= q_{i,j}^n \\ q_{i,j}^{(1)} &= q_{i,j}^n + \alpha_1 \Delta t R[q_{i,j}^{(0)}] \\ q_{i,j}^{(2)} &= q_{i,j}^n + \alpha_2 \Delta t R[q_{i,j}^{(1)}] \\ q_{i,j}^{(3)} &= q_{i,j}^n + \alpha_3 \Delta t R[q_{i,j}^{(2)}] \\ q_{i,j}^{(4)} &= q_{i,j}^n + \alpha_4 \Delta t R[q_{i,j}^{(3)}] \end{aligned} \tag{18}$$

The second-order algorithm of Jameson and Baker[48] is applied. This corresponds to the following coefficient values: $\alpha_1 = \frac{1}{4}$, $\alpha_2 = \frac{1}{3}$, $\alpha_3 = \frac{1}{2}$, $\alpha_4 = 1$. This algorithm is convenient to program and no intermediate solution needs to be stored. Its numerical properties have been studied in detail in Ref. 49. This scheme is stable for a Courant number $C_N \leq 2\sqrt{2}$ if the dissipative effects are small enough.[50] Moreover, the dissipation terms are frozen at the level (0) to reduce the computational effort required for their evaluation at each stage of the RK scheme.

Convergence Acceleration to Steady State

Attainment of the steady state can be accelerated by the use of a spatially variable time step, with the present algorithm remaining stable for relatively high values of the Courant number. At each grid point the solution is allowed to advance in time following the criterion

$$\Delta t_{i,j} = C_N \sigma_{i,j}^{-1} \tag{19}$$

where $\sigma_{i,j}$ is the spectral radius scaling defined as

$$\sigma_{i,j} = |U| + c\sqrt{\xi_x^2 + \xi_y^2} + |V| + c\sqrt{\eta_x^2 + \eta_y^2} \tag{20}$$

In this equation, the Courant number C_N is either constant everywhere $C_N = C_{N\max}$, or it satisfies the following law:

$$C_N = \min\left(\frac{\chi}{\text{residual}^n}, C_{N\max} \right) \tag{21}$$

where residual^n is defined by

$$\text{residual}^n = \frac{\max_{i,j} |(\rho_t)_{i,j}^n|}{\max_{i,j} |(\rho_t)_{i,j}^0|} \tag{22}$$

In practice, $\chi = 2$.

The use of the law (21) increases the robustness of the code which is required to get past the initial transients.

Convergence can also be accelerated by the use of the implicit residual average technique proposed by Jameson and Baker.[48] This step is introduced to give an additional implicit character to the general algorithm, and thereby increase the maximum allowable Courant number. It also has the benefit of smoothing the high-frequency variations of the residual. In the present application, it is sufficient to apply the smoothing at the second and fourth stages of the RK scheme.

Regarding the treatment of the boundary conditions at the body surface, updated values for the surface pressure are obtained from Eq. (13) by central differencing the ξ derivatives, forward differencing the η derivatives, and solving tridiagonal system of equations for p along the body surface.

Table 1 Effect of the grid size on the computed value Δp

Grid size	$\Delta\xi_{min}$, m[a]	$\Delta\eta_{min}$, m[b]	ξ_{max}, m[c]	η_{min}, m[d]	Δp, Pa
61 × 61	2.00×10^{-5}	2.00×10^{-5}	0.086	0.078	46,802
91 × 91	1.25×10^{-5}	1.25×10^{-5}	0.086	0.078	46,712
61 × 66	2.00×10^{-5}	2.00×10^{-5}	0.086	0.156	46,762

[a]Effective minimum grid spacing in the ξ direction.
[b]Effective minimum grid spacing in the η direction.
[c]Downstream boundary location.
[d]Far-field boundary location.

Table 2 Comparison for the freestream velocity between the numerical value and the theoretical or semiempirical approximations deduced from the computed pressure difference, $M_\infty = 0.1$, $p_\infty = \frac{1}{2}$, atm

		Numerical	Velocity U_∞, m/s deduced from		
p_∞, atm	T_∞, K	value U_∞, m/s	$\Delta p_3 = \Delta p$ and Eq. (3)	$\Delta p_2 = \Delta p$ and Eq. (2)	$\Delta p_1 = \Delta p$ and Eq. (1)
1.0	300	34.79	34.79	34.82	34.86
1.0	2000	87.81	88.35	88.88	89.00
1.0	3500	115.95	117.41	119.03	119.19
1.0	5000	145.09	149.26	152.47	152.68
0.5	300	34.79	34.79	34.85	34.89
0.5	2000	87.81	88.81	89.85	89.97
0.5	3500	116.58	119.11	122.43	122.60
0.5	5000	145.48	152.58	158.64	158.88
0.3333	300	34.79	34.79	34.88	34.92
0.3333	2000	87.81	89.23	90.77	90.89
0.3333	3500	117.00	120.41	125.42	125.60
0.3333	5000	145.70	155.50	164.24	164.50
0.25	300	34.79	34.79	34.91	34.96
0.25	2000	87.81	89.72	91.74	91.87
0.25	3500	117.31	121.65	128.30	128.49
0.25	5000	145.87	158.66	169.92	170.21

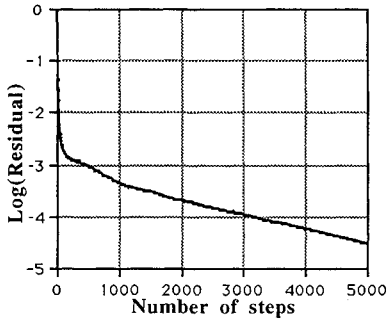

Fig. 3 Time history of density residual.

Results and Discussion

The Navier-Stokes solver described above is applied to a variety of flowfields around the pitot tube. The radius of curvature of the tube at the impact point is 0.002 m. The potential flow solution serves as initial condition for the calculation. First we present the results of a simulation of a transonic air plasma flow around a pitot tube whose surface temperature is kept constant at $T_p = 300$ K. The freestream conditions are $M_\infty = 0.80$, $p_\infty = 1$ atm (0.101325 MPa), and $T_\infty = 5000$ K. The computation is performed on the 61 × 61 base grid with effective minimum grid spacing $\Delta\xi = 2 \times 10^{-5}$ m, $\Delta\eta = 2 \times 10^{-5}$ m, and maximum Courant number of 4.

For the present calculation, the present method requires 5000 time steps to converge, i.e., to satisfy simultaneously the following convergence criteria:

$$\text{residual}^n < 10^{-4}$$

$$\frac{\Delta p^{n+1} - \Delta p^n}{\Delta p^{n+1}} \leq 10^{-5}$$

where Δp is the numerical value of the difference between the impact pressure and the freestream pressure. This takes approximatively 1 h on an IBM 3090-VF computer.

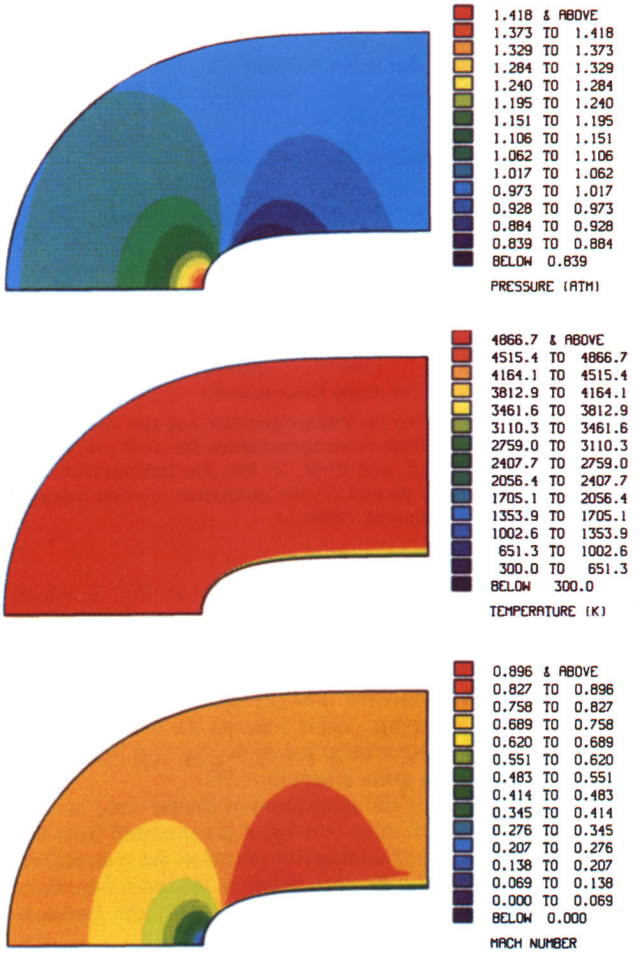

Fig. 4 Detail showing pressure, temperature, and Mach number shaded contours in the vicinity of the body nose.

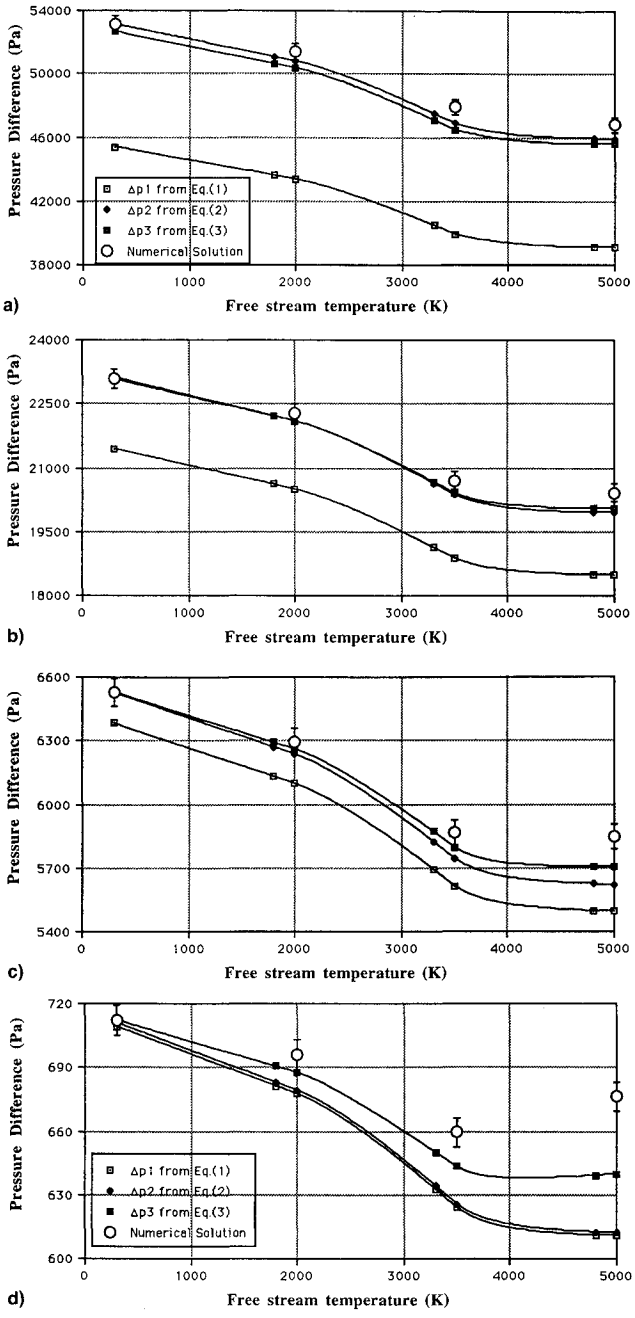

Fig. 5 Difference between the impact pressure and the atmospheric freestream pressure vs freestream temperature for a) $M_\infty = 0.8$, b) $M_\infty = 0.55$, c) $M_\infty = 0.3$, and d) $M_\infty = 0.1$. For information only, the segments which are plotted on the numerical solution markers represent 2% of the computed value.

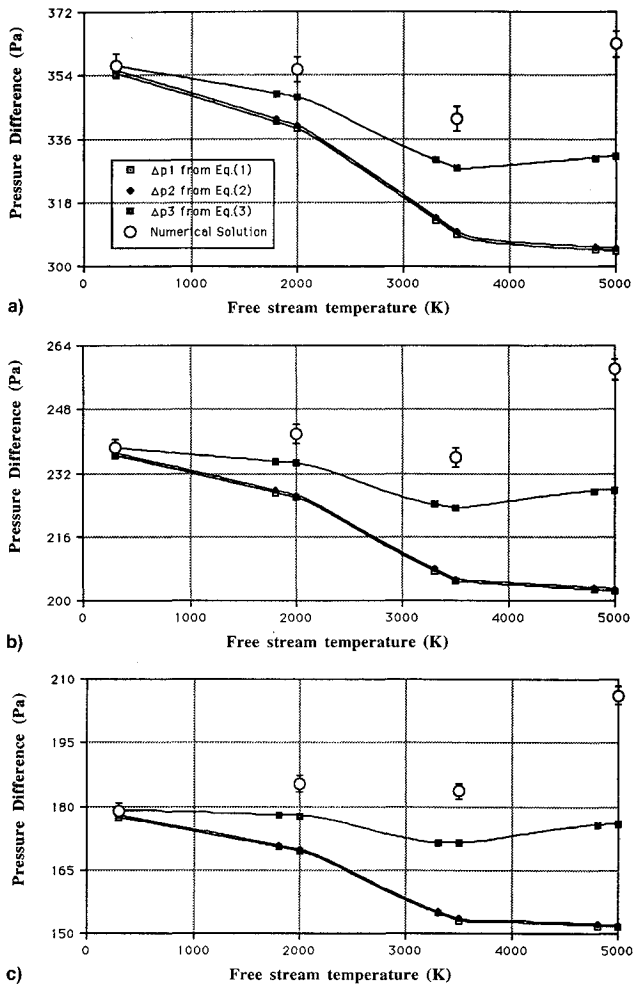

Fig. 6 Pressure difference vs freestream temperature for $M_\infty = 0.1$ and a) $p_\infty = \frac{1}{2}$, b) $p_\infty = \frac{1}{3}$, and c) $p_\infty = \frac{1}{4}$ atm. For information only, the segments which are plotted on the numerical solution markers represent 2% of the computed value.

Numerical convergence history is shown in Fig. 3, which plots the logarithm of the normalized residual of density vs the number of time steps.

In order to judge the accuracy of the numerical results a grid refinement is performed. The present test case is recomputed with 91 × 91 points. Table 1 shows the computational details and the Δp comparison for both fine and base grids. The solution for both grids is within 0.2%.

The effect of varying the placement of the far-field boundary is also investigated. A 61 × 66 grid is generated from the 61 × 61 base grid by just adding five points in the η direction. That leads to double the distance between the outer boundary and the body surface. As shown in Table 1, the pressure difference is nearly identical for the two grids.

As the difference in Δp is relatively small for all three grids, the 61 × 61 base grid is used for all the computations.

Pressure, temperature, and Mach number contours in the vicinity of the body nose are shown in Fig. 4. A thermal boundary layer surrounding the probe is created. As argued by Smith and Churchill,[32] and observed experimentally by Hare[23] for low-pressure plasmas, the presence of this layer could affect the magnitude of the measured impact pressure. To verify these assertions and give some idea of the magnitude of the effect, a comparison is made between the computed values of Δp and those obtained from Eqs. (1–3) for T_p = 300 K and freestream temperature in the range 300–5000 K as the freestream Mach number and pressure vary. The results of the comparison are summarized in Figs. 5 and 6. Hereafter, Δp_1, Δp_2, and Δp_3 represent the pressure differences deduced from the Eqs. (1), (2), and (3), respectively.

Effect of the Freestream Mach Number

By comparing in Fig. 5 the pressure differences for p_∞ = 1.0 atm and M_∞ = 0.8, 0.55, 0.3, and 0.1 (diagrams a–d), it can be seen that for all these configurations the computed pressure difference Δp is higher than the other ones. Putting to one side the specific transonic case (Fig. 5a), the solution given by the Carleton's relation is generally the closest to the computed value. Furthermore, the departure of Δp from Δp_3 increases as the freestream temperature increases and the freestream Mach number decreases. For M_∞ = 0.1 and T_∞ = 5000 K, when the temperature difference between the gas and the probe is the highest, a 5.43% deviation of Δp from Δp_3 is observed.

Figure 5d reveals slope changes of Δp and Δp_3 at about T_∞ = 3500–4000 K for M_∞ = 0.1, while for higher Mach number they are ever-decreasing functions of T_∞.

Effect of the Freestream Pressure

Diagrams a–c in Fig. 6 correspond to $p_\infty = \frac{1}{2}, \frac{1}{3}, \frac{1}{4}$ atm, respectively, for M_∞ = 0.1. For such conditions compressibility effects are negligible, and in this case Δp_1 and Δp_2 are very close together. The effects of viscosity, heat transfer, and reactivity on the impact pressure may in this way be distinguished from the compressible effects.

The slope change of the curves Δp and Δp_3, observed previously in Fig. 5d, becomes more pronounced. Both of the curves pass through a minimum for T_∞ = 3500 K. At T_∞ = 5000 K, the computed value Δp deviates from the Carleton pressure difference Δp_3 by

9.65% for $p_\infty = \frac{1}{2}$ atm

13.22% for $p_\infty = \frac{1}{3}$ atm

17.15% for $p_\infty = \frac{1}{4}$ atm

We can see that these values indicate that the departure between the value deduced from Carleton's relation (Δp_3), and the value resulting from the numerical calculation (Δp), increases significantly as the freestream decreases. This tends to confirm the restraints raised by Hare, especially if one wants, as he did, to take measurements for very low freestream pressure.

Since impact tubes are frequently used to determine the velocity of a flowing gas, it was interesting to evaluate, for a Δp given by the numerical model, what values of velocity the use of Eqs. (1), (2), or (3) might lead to. These values are compared to the velocity value used as the initial condition in the numerical calculation of the Δp. The results are presented in Table 2. A maximum 17% deviation of the initial value U_∞ from the Bernoulli solution can be seen.

Conclusions

The principal goal of this research was the development of a numerical tool in order to relate the pressure sensed by a cooled pitot tube in a plasma flow to the freestream velocity. The solution algorithm is based on the use of a multistage time-stepping procedure combined with the conventional second-order spatial discretization. The numerical results indicate quite clearly under which conditions and in which measure the classical relations (Bernoulli, "compressible," and Carleton) are put into question when high temperature difference between the plasma jet and the probe occurs. The departures of the computed impact pressure from those deduced from these classical relations are evaluated.

All these results taken together show the influence of the real-gas effects (e.g., viscosity, conduction, atomic recombination) and compressibility effects. On the whole, the values deduced using Carleton's relation are the closest to the results obtained from the numerical model contained in this article. This is not surprising because out of three relations looked at, it is his semiempirical relation which best takes account of real-gas effects.

Within the range of the atmospheric pressure, we consider that Carleton's relation can be validly employed to link the impact pressure to the freestream flow conditions, and thus to deduce the freestream velocity of the plasma flow. However, as soon as the pressure is lower than the atmospheric pressure, we observe that the values given by Carleton's relation deviates considerably from our calculated values. This tendency confirms the experimental results of Hare,[23] which concern low-pressure plasma flows.

Acknowledgment

This research work was sponsored by Electricité de France, Paris, France.

References

[1]Bouvier, A., and Jestin, L., "R&D at EDF into the Industrial Application of Plasma Generators," *Plasma Jets*, edited by O. P. Solonenko and A. I. Fedorchenko, VSP, Utrecht, The Netherlands, 1990, pp. 463–472.

[2]Shohet, J. L., "Plasma Processing and Technology in Industry," AIAA Paper 92-3011, July 1992.

[3]Partiot, A., "Plasmas Torches," *Revue Aerospatiale*, No. 93, 1992, pp. 30–37.

[4]Viollet, P. L., Gabillard, M., and Mechitoua, N., "Modélisation Tridimensionnelle des Plasmas Thermiques en Ecoulement," *Revue de Physique Appliquée*, Vol. 25, 1990, pp. 843–857.

[5]Simonin, O., Delalondre, C., and Viollet, P. L., "Modelling of Thermal Plasma and Electric Arc Column," *Proceedings of the 10th International Symposium on Plasma Chemistry*, edited by U. Ehlemann, H. G. Lergon, and K. Wiesemann, Bochum, Germany, 1991.

[6]Gabillard, M., Lana, F., and Jestin, L., "Comparison Between Experimental and Numerical Calculation Results for the Wall Temperature Reached in a Mixed Flow of Plasma and Air at 9200 C," *Proceedings of the 9th International Symposium on Plasma Chemistry*, edited by B. Agostino, Vol. 3, Bari, Italy, 1989, pp. 1759–1764.

[7]Cahen, C., and Spiberg, P., "Laser Diagnosis Inside a ZMW Plasma Generator," *Plasma Jets*, edited by O. P. Solonenko and A. I. Fedorchenko, VSP, Utrecht, The Netherlands, 1990, pp. 149–161.

[8]Katta, S., Lewis, J. A., and Gauvin, W. H., "A Plasma Calorimetric Probe," *Review of Scientific Instrumentation*, Vol. 44, No. 10, 1973, pp. 1519–1523.

[9]Grey, J., Jacobs, P. F., and Sherman, M. P., "Calorimetric Probe for the Measurement of Extremely High Temperatures," *Review of Scientific Instrumentation*, Vol. 33, No. 7, 1962, pp. 738–741.

[10]Grey, J., "Sensitivity Analysis for the Calorimetric Probe," *Review of Scientific Instrumentation*, Vol. 34, No. 8, 1963, pp. 857–859.

[11]Grey, J., "Thermodynamic Methods of High Temperature Measurement," *ISA Transactions*, Vol. 4, No. 2, 1965, pp. 102–115.

[12]Chludzinski, G. R., Kadlec, R. H., and Churchill, S. W., "Energy Transfer to Probes in Argon-Nitrogen Plasmas," *AIChE Journal, Symposium Series*, No. 2, 1965, pp. 93–98.

[13]Vassalo, F. A., "Miniature Probes for High Temperatures Gas Streams," Aeronautical Research Labs. Rept. 66-0115, 1965.

[14]Grey, J., Sherman, M. P., Williams, P. M., and Fradkin, D. B., "Laminar Arcjet Mixing and Heat Transfer: Theory and Experiments," *AIAA Journal*, Vol. 4, No. 6, 1966, pp. 986–993.

[15]Grey, J., and Jacobs, P. F., "Cooled Electrostatic Probe," *AIAA Journal*, Vol. 5, No. 1, 1967, pp. 84–90.

[16]Massier, P. F., Back, L. H., and Roschke, E. J., "Heat Transfer and Laminar Boundary-Layer Distributions in an Internal Subsonic Gas Stream at Temperatures Up to 13,900 Deg R," *Journal of Heat Transfer, American Society of Mechanical Engineers Transactions*, 1967, pp. 83–90.

[17]Voropaev, A. A., Dresvin, S. V., and Klubnikin, V. S., "Measurement of Plasma Flow Velocity with a Total Head Tube," *Teplofizika Vysokhikh Temperatur*, Vol. 7, No. 4, 1969, pp. 633–640.

[18]Carleton, F. E., "Flow Patterns in a Confined Plasma Jet," Ph.D. Dissertation, Univ. of Michigan, Ann Arbor, MI, 1970.

[19]Cox, J. B., and Weinberg, F. J., "On the Behaviour of Enthalpy Probes in Fluctuating Temperature Environments," *Journal of Physics D, Applied Physics*, Vol. 4, 1971, pp. 877–881.

[20]Carleton, F. E., and Kadlec, R. H., "Impact Tube Gas Velocity Measurement at High Temperatures," *AIChE Journal*, Vol. 18, No. 5, 1972, pp. 1065–1067.

[21]Dresvin, S. V., and Klubnikin, V. S., "Plasma Temperature Measurements Using an Enthalpy Probe," *Teplofizika Vysokhikh Temperatur*, Vol. 13, No. 2, 1975, pp. 433–435.

[22]Pakhomov, E. P., and Yartsev, M. I., "Measurement of the Velocity of Plasma Flow by Means of a Total Head Pressure Probe," *Teplofizika Vysokhikh Temperatur*, Vol. 14, No. 3, 1976, pp. 598–605.

[23]Hare, A. L., "Velocity Measurement in Plasma Flows Using Cooled Pitot Tubes: An Unsolved Problem," *Proceedings of the 3rd International Symposium on Plasma Chemistry*, G3.1, Limoges, France, 1977.

[24]Hare, A. L., "Enthalpy Probes: A Contribution to Theory of Operation," *Proceedings of the 3rd International Symposium on Plasma Chemistry*, G3.1, Limoges, France, 1977.

[25]Brossa, M., and Pfender, E., "Probe Measurements in Thermal Plasma Jets," *Plasma Chemistry and Plasma Processing Journal*, Vol. 8, No. 1, 1988, pp. 75–90.

[26]Capetti, A., and Pfender, E., "Probe Measurements in Argon

Plasma Jets Operated in Ambient Argon," *Plasma Chemistry and Plasma Processing Journal*, Vol. 9, No. 2, 1989, pp. 329–341.

[27]Stefanovic, P., Pavlovic, P., and Jankovic, M., "High Sensitive Calorimetric Probe for Diagnostics Thermal Plasma at the Exit of Electric Arc Heater," *Proceedings of the 3rd International Symposium on Plasma Chemistry*, edited by B. Agostino, Vol. 1, Bari, Italy, 1989, pp. 314–318.

[28]Barker, M., "On the Use of Very Small Pitot Tubes for Measuring Wind Velocity," *Proceedings of the Royal Society*, Series A, No. 101, 1922, p. 435.

[29]MacMillian, F. A., "Viscous Effects on Pitot Tubes at Low Speeds," *Journal of the Royal Aeronautics Society*, No. 58, 1954, p. 570.

[30]Schowalter, W. R., and Blaker, G. E., "On the Behavior of Impact Probes at Low Reynolds Numbers," *Journal of Applied Mechanics*, No. 28, 1961, p. 136.

[31]Sherman, F. S., "New Experiments on Impact-Pressure Interpretation in Supersonic and Subsonic Rarefied Air Streams," National Advisory Committee for Aeronautics, TN 2995, 1953.

[32]Smith, D. L., and Churchill, S. W., College of Engineering, Univ. of Michigan, Tech. Rept. ORA Project 05607, Ann Arbor, MI, 1965.

[33]Porterie, B., Loraud, J. C., Larini, M., and Jestin, L., "Numerical Simulation of Subsonic Air Plasma Flow About a Cooled Pitot Tube," AIAA Paper 92-4004, July 1992.

[34]Peyret, R., and Viviand, H., "Computation of Viscous Compressible Flows Based on the Navier-Stokes Equations," AGARD-AG-212, 1975.

[35]Pateyron, B., Elchinger, M. F., Delluc, G., and Aubreton, J., "Banque de Données de l'Université et du CNRS," edited by F. Libmann Assoc., Paris, 1989.

[36]Danton, C., and Dudeck, M., "Concentrations à l'Equilibre dans un Mélange Azote-Oxygène," Laboratoire d'Aérothermique de Meudon, France, 1986.

[37]Brinkley, S. R., *Journal of Chemical Physics*, Vol. 28, 1947, p. 107.

[38]Stull, D. R., and Prophet, H., "JANAF Thermochemical Tables," 2nd ed., NSRDS-NBS37, June 1971.

[39]Vincenti, W. G., and Kruger, C. H., Jr., *Introduction to Physical Gas Dynamics*, Wiley, New York, 1967.

[40]Palmer, G., "An Improved Flux-Split Algorithm Applied to Hypersonic Flows in Chemical Equilibrium," AIAA Paper 88-2693, June 1988.

[41]Jameson, A., Schmidt, W., and Turkel, E., "Numerical Solution of the Euler Equations by Finite Volume Methods Using Runge-Kutta Time-Stepping Schemes," AIAA Paper 81-1259, June 1981.

[42]Jameson, A., "Transonic Aerofoil Calculations Using the Euler Equations," *Numerical Methods in Aeronautical Fluid Dynamics*, edited by P. L. Roe, Academic Press, New York, 1982.

[43]Jameson, A., "Successes and Challenges in Computational Aerodynamics," AIAA Paper 87-1184, June 1987.

[44]Martinelli, L., Jameson, A., and Grasso, F., "A Multigrid Method for the Navier-Stokes Equations," AIAA Paper 86-0208, Jan. 1986.

[45]Martinelli, L., and Jameson, A., "Validation of a Multigrid Method for the Reynolds Averaged Equations," AIAA Paper 88-0414, Jan. 1988.

[46]Satofuka, N., Morinishi, K., Tamaki, T., and Shimizu, A., "Computation of Two-Dimensional Transonic Cascade Flow Using a New Navier-Stokes Solver," AIAA Paper 86-1381, June 1986.

[47]Pulliam, T. H., "Artificial Dissipation Models for the Euler Equations," *AIAA Journal*, Vol. 24, No. 12, 1986, pp. 1931–1940.

[48]Jameson, A., and Baker, T. J., "Multigrid Solution of the Euler Equations for Aircraft Configurations," AIAA Paper 84-0093, Jan. 1984.

[49]Yu, T. S., Tsai, L. P., and Hsieh, K. C., "Runge-Kutta Methods Combined with Compact Difference Schemes for the Unsteady Euler Equations," AIAA Paper 92-3210, July 1992.

[50]Fletcher, C. A. J., *Computational Techniques for Fluid Dynamics*, Springer Series in Computational Physics, Vol. II, Springer-Verlag, Berlin, 1988, p. 408.